Research article

Markus Giehl*, Lukas T. Hiller and Cornelius Neumann

Manufacturing of volume holographic cell arrays for usage with uncollimated LEDs in automotive applications

https://doi.org/10.1515/aot-2020-0037
Received June 30, 2020; accepted October 13, 2020;
published online November 5, 2020

Abstract: Holograms have found their use as optical elements in a variety of applications. Yet using them with incoherent and divergent lightsources like LEDs proves difficult, as their characteristics need to be simulated by lasers during manufacturing to get a correct reconstruction of the desired light distribution. We present a new setup to allow for a high flexibility during the manufacturing process, which is able to produce volume holographic cell arrays (VCAs) that can be illuminated directly with uncollimated LEDs. Results are presented for the case of reflection holograms.

Keywords: automotive; holography; LED illumination; manufacturing; photopolymer.

1 Introduction

Since the holographic principle was shown by Gabor [1], holograms have found their way from a purely scientific application to a wide range from 3D imaging and microscopy [2] to head-up displays, copy protection and tailored optical elements.

With the introduction of new holographic photopolymers [3] in form of thin films, an integration of volume holographic optical elements (vHOEs) in automotive applications is conceivable [4]. Furthermore, the optical designer has the ability to provide different optical functions with the element. This is because vHOEs consist of a volume grating, defined by a refractive index modulation of the photopolymer. These gratings act in a similar fashion as a crystal lattice does for X-rays and scatter the incident light. The scattered waves interfere constructively and reflect light when Bragg's condition

$$2d \sin\theta = n\lambda \tag{1}$$

[5] is met, with glancing angle α, lattice plane distance d and wavelength λ. A coupled wave analysis of condition, Equation (1), allows for a calculation of the angular and wavelength sensitivities of the volume grating [6]. The material stays transparent when it is illuminated by an angle or wavelength differing from Equation (1), which may give the possibility to provide different optical functions within the same area, realize barely visible optical elements or simply achieve optical functions with very thin elements. First approaches to collimating optical elements are presented in the studies by Bruder et al. [7] and Mintz et al. [8], which use a point-source during exposure of the holographic film. The main difficulty to achieve this for different kinds of LEDs lies in the forming of a reference beam, capable of representing their Lambertian characteristics. That means each new illumination system would require a specific manufacturing setup, as the reference beam has to be formed accordingly. But achieving such large divergence angles with lasers is nearly impossible with common lenses and generating point sources by diffraction at small apertures does not give accurate results as the characteristics strongly depend on the lightsource used [9, 10].

Here we present a new setup, which allows to manufacture computer-generated matrix holograms [11] with a very high flexibility regarding the reference angle during the printing process. Therefore, changes in the illumination setup can be addressed without changing elements in the holographic printer. As we use volume holograms, we call them volume holographic cell arrays (VCAs).

*Corresponding author: Markus Giehl, L-LAB Research Institute for Automotive Lighting and Mechatronics, Lippstadt, Germany, E-mail: markus.giehl@l-lab.de
Lukas T. Hiller, L-LAB Research Institute for Automotive Lighting and Mechatronics, Lippstadt, Germany
Cornelius Neumann, Karlruher Institute of Technology, Karlsruhe, Germany

2 Hologram printer

2.1 Illumination system

Our goal is to print holograms suitable for the general lighting system depicted in Figure 1. A VCA is illuminated by a nearby LED with lightrays ϱ coming from the LED. The hologram is supposed to reflect the rays σ to achieve the desired light distribution on the screen. The rays are described in spherical coordinates with elevation angle θ and azimuthal angle φ. The collimation of σ would, for instance, require the reference beam directions to be identical to ϱ for each matrix element and the object beam directions σ to be parallel to each other.

2.2 General setup

To achieve the desired flexibility in printing VCAs with a wide range of different reconstruction angles, we propose a new setup that allows to produce transmission and reflection holograms. A principle sketch is shown in Figure 2. The setup contains different lasers according to the desired wavelength sensitivity of the holographic film.

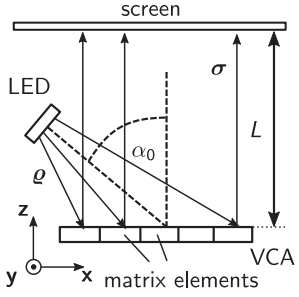

Figure 1: Illumination system consisting of an LED with lightrays ϱ and the VCA, which reflects the incident light into direction σ.

The laser beams are widened up, collimated and limited by a much smaller rectangular aperture A_R to match the active area of the spatial light modulator (SLM) and get a homogenous intensity distribution from the Gaussian profile of the laser intensity. Dicroitic mirrors reflect the laser beams onto a common optical axis. After that, the beams get split up by a beam splitter BS_1 into the reference beam (positive x-direction) and the object beam (negative x-direction). As the VCAs are computer-generated, the calculated phase information of the object beam is displayed on an SLM and depicted on the holographic film by lenses f_{O_1} and f_{O_2} with magnitude $s = 0, 1$. The reduction is necessary to decrease the structural size of each cell. Unwanted diffraction orders are blocked by aperture A_O. In the reference beam, the mapping of aperture A_R on the film is covered by a variable lens system f_R^* and the parabolic mirror itself, which acts as the second lens of a $4f$ system.

2.3 Parabolic reflector

The primary feature of the setup is the large parabolic mirror, which acts as a focusing and beam steering element. By addressing different positions parallel to the optical axis o_P, large angle variations of $\theta \approx [5, 70]$ deg (in the x-z plane in Figure 2) and $\varphi \approx [5, 175]$ deg (in the x-y plane in Figure 6) can be achieved without changing the focus position. A microscopy stage is positioned at the center of the reflector to change the position of the holographic film in the x-y plane. Together with a movable mirror M_{P_2}, it is possible to change the reference angle at different positions of the holographic film. Following the work of Bruder et al. [12], the power density ratio of the laser beams at the focus point inside the holographic film should be equal to one. To ensure this, several corrections must be made that arise from the parabolic mirror principle.

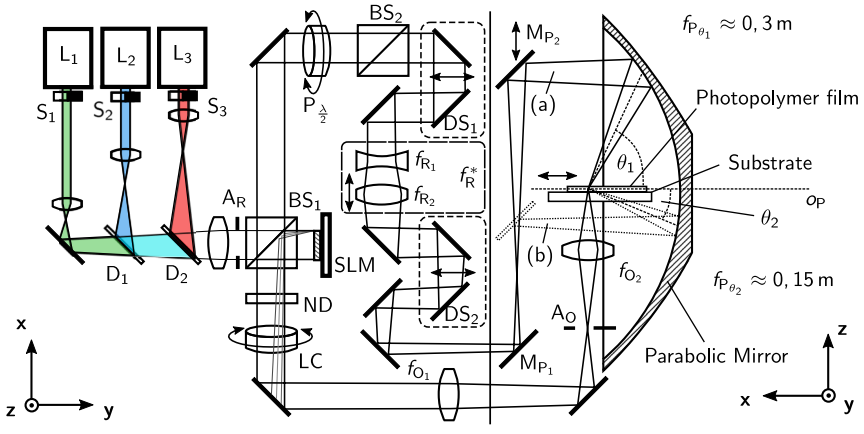

Figure 2: Principle sketch of the hologram printer. An SLM is used to apply the computer-generated VCA phase images to the object beam. The reference beam is steered by a large parabolic reflector to achieve a wide range of reference angles, which results in focal length changes depending on the reflector position. In example (a), printing of a reflection hologram with acute angle and $f_P \approx 0, 30$ m and (b), a transmission hologram with flat angle and $f_P \approx 0, 15$ m is observed.

2.3.1 Optical path correction

The reference angle is changed for each cell, which means that the reflector's focal length changes as well. In Figure 2, two cases are depicted: (a) Manufacture of a reflection hologram with elevation θ_1 results in a focal length of ≈300 mm, while a small angle θ_2 in case (b) for a transmission hologram gives a focal length of ≈150 mm. Independent of the reference angle, the size of the focus needs to be constant and the 4*f* relation has to be preserved. This means that the focal length of lens system $f_R^\star$and the optical path between A_R, $f_R^\star$, and the parabolic mirror have to be modified accordingly.

The optical path lengths depend on those of the reference beam in the given setup, however, we will describe the procedure exemplary for our assembly. The focal length of the mirror lies roughly between 150 mm and 300 mm, which means the optical paths before and after $f_R^\star$ must cover $1/s = 10$ times the mirror focal length for a magnification of $s = 0, 1$. Figure 3 shows a pseudocolor plot of the effective path length that has to be covered by delay stage DS_2 after $f_R^\star$. Taking into account that the laser beam travels along the *x* and *y* directions before coupling into the reflector along *z*, the resulting path length becomes asymmetrical and is not identical to the focal length anymore.

2.3.2 Focal length correction

For the calculation of the lens system, one can make use of the matrix formalism [13, p. 26–32] in Figure 4.

The effective focal length $f_R^\star$ is calculated by propagating a collimated beam ray

$$r_0 = \begin{pmatrix} r_0 \\ \phi_0 \end{pmatrix} = \begin{pmatrix} r_0 \\ 0 \end{pmatrix} \tag{2}$$

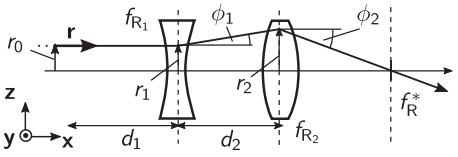

Figure 4: Illustration of the matrix description of the lens system in the reference beam.

through the system consisting of a thin diffusion lens f_{R_1} and a thin converging lens f_{R_2} in distance d_2 to each other. This yields the complete matrix equation

$$\boldsymbol{r}_2 = \boldsymbol{L}(f_2) \cdot \boldsymbol{T}(d_2) \cdot \boldsymbol{L}(f_1) \cdot \boldsymbol{T}(d_1) \cdot \boldsymbol{r}_0 \tag{3}$$

and $f_R^\star$ can be calculated from r_2 with

$$f^* = \frac{\tan(-\phi_2)}{r_2}. \tag{4}$$

A suitable lens system is depicted in Figure 5, providing the complete range of focal lengths by moderately changing d_2. In addition, the back focal length, which is crucial for the path of delay stage DS_1, progresses in the same way with a constant offset.

2.3.3 Polarization correction

Beams parallel to the optical axis of a parabolic mirror have a common focus point. We use this feature to vary the angle of the reference beam, but as illustrated in Figure 6, its polarization vector p_R changes as well with regard to the object beam polarization p_O. This change needs to be compensated to match the polarizations of the respective beams in the substrate plane. Otherwise, the interference pattern recorded in the photopolymer film will be of low contrast, resulting in a low efficiency of the VCAs. For maximum contrast, s-polarization (Figure 6) is necessary. Changing the reference beam would result in p-polarized beams, which is why the object beam has to be modified.

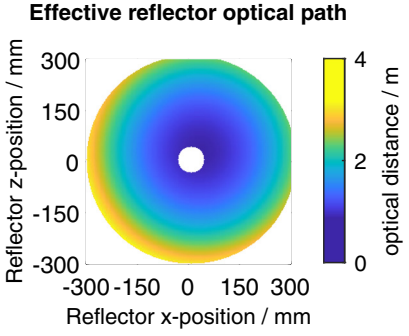

Figure 3: Resulting optical path of the reference beam, depending on the lateral reflector position.

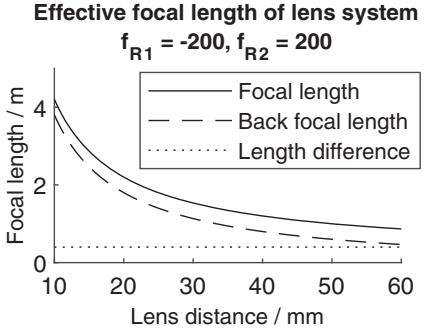

Figure 5: Effective focal length and back focal length of the lens system for different lens distances.

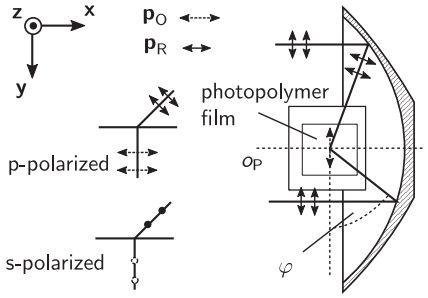

Figure 6: Polarization changes caused by the parabolic mirror with reference beam polarization p_R and object beam polarization p_O.

To match the polarizations, p_R is calculated in the substrate plane and the liquid crystal (LC) (Figure 2) is used to adjust the polarization of the object beam. The element is configured as a $\lambda/2$ wave plate for the specific wavelength used during the writing process. The polarization is then adjusted by rotating the LC depending on the reflector position.

Equation (5) shows an implicit representation of the parabolic mirror in the coordinate system, where the x axis is the axis of rotational symmetry. The parameter a in Equation (6) depends on focal length f. The normal vectors $\vec{n}$ of the parabolic mirror are given by the gradient of p in Equation (7).

$$p = -a\left(z^2 + y^2\right) + x = 0 \tag{5}$$

$$a = \frac{1}{4f} \tag{6}$$

$$\hat{n} = \frac{\vec{n}}{\left|\vec{n}\right|} = \frac{\vec{\nabla}\,(p)}{\left|\vec{n}\right|} = \frac{(-2az, -2ay, 1)}{\sqrt{4a^2\left(z^2 + y^2\right) + 1}} \tag{7}$$

The reference beam is approximated by a plane electromagnetic wave $\vec{E}$, Equation (8). Since there is only linear polarization in this case, it is sufficient to consider the amplitude vector $\vec{E}_0$, Equation (9) for further calculations.

$$\vec{E} = \vec{E}_0\ \exp\left(-\mathrm{i}\left(\vec{k}\vec{r} - \omega t\right)\right) \tag{8}$$

$$\vec{E}_0 = (E_x, E_y, E_z) \tag{9}$$

To calculate the polarization of the reference beam in the substrate plane, the polarization vector $\vec{E}_0$ of the reference beam needs to be mirrored at a line $\vec{g}$, Equation (10) along the normal vector $\hat{n}$ of the parabolic mirror, Equation (7), and is then projected onto the substrate plane. For the calculation of the mirrored polarization vector $\vec{E}'_0$, a shifted coordinate system S' is chosen, where the origin is the intersection of the reference beam and the parabolic mirror. In this case, $\vec{E}'_0$ can be calculated by mirroring point ($\vec{E}_0$) at line ($\vec{g}$). A plane through $\vec{E}_0$ and perpendicular to $\vec{g}$ is cut with $\vec{g}$ to find the parameter $t = t_0$, Equation (11).

$$\vec{g} = t\hat{n} \tag{10}$$

$$t_0 = \langle \hat{n}, \vec{E}_0 \rangle \tag{11}$$

With $\vec{E}_g = \vec{g}\,(t_0)$, the mirrored polarization vector $\vec{E}'_0$, Equation (11), is found.

$$\vec{E}'_0 = \vec{E}_0 + 2\left(\vec{E}_g - \vec{E}_0\right) = 2\,\langle\, \hat{n}\vec{E}_0 \,\rangle\ \hat{n} - \vec{E}_0 \tag{12}$$

Now $\vec{E}'_0$ needs to be projected on the substrate plane, which is the x-y plane in the coordinate system S. The projected vector is given by $\vec{E}'_{0\,\mathrm{proj}}$, Equation (12).

$$\vec{E}'_{0\,\mathrm{proj}} = \left(\vec{E}'_x, \vec{E}'_y, 0\right) \tag{13}$$

The angle between the polarization vectors of the object beam $\vec{E}_O$ and the projected reference beam $\vec{E}'_{0\,\mathrm{proj}}$ is given by Equation (14).

$$\cos(\gamma) = \frac{\langle \vec{E}_0\, \vec{E}'_{0\,\mathrm{proj}} \rangle}{\left|\vec{E}_0\right| \left|\vec{E}'_{0\,\mathrm{proj}}\right|} \tag{14}$$

Rotating the LC-element in the object beam's path by $\gamma/2$ matches the polarization of the object beam to the reference beam.

2.3.4 Correction of the beam ratio

Finally, the beam ratio itself has to be modified, since the reference beam is attenuated while entering into the substrate due to Fresnel reflection for large angles. In Equation (15), the transmission coefficient t_s for the reflection of perpendicular polarized light is shown [13, p. 246]

$$t_s = \frac{2n_1\ \cos(\alpha)}{n_1 \cos(\alpha) + \sqrt{n_2^2 - n_1^2\ \sin^2(\alpha)}} \tag{15}$$

In this work, $n_1 \approx 1$ is the refractive index of air, n_2 the refractive index of the holographic foil and $\alpha = \frac{\pi}{2} - \theta$, the angle of the reference beam. For the collimation setup in Figure 1, the angle of incidence is small for the object beam, and the progression of the Fresnel reflection for the object beam is neglected. Since there are two interfaces for the

object beam propagating through the foil (air–glass, glass–foil), the transmission coefficient is approximated with $t_{obj} \approx 0,9$.

Because of Equation (15), the beam ratio inside the photopolymer film decreases with elevation angle θ, however, for good results a ratio of BR = 1 in the film is needed [14, p. 10] with

$$\mathrm{BR} = \frac{P_{obj}}{P_{ref}} \frac{t_{obj}}{t_{ref}} \approx \frac{P_{obj}}{P_{ref}} \frac{0,9}{t_s}. \tag{16}$$

The beam ratio is corrected by decreasing the object beam power with a neutral density filter ND (Figure 2) and adapting the reference beam power by rotation of halfwave plate $P_{\lambda/2}$, which is positioned ahead of a polarizing beamsplitter BS_2.

3 Results

3.1 Evaluating correction measures

Before printing, the used material needs to be characterized and the described correction measures need to be evaluated. For the given application, we use the Covestro Bayfol HX200 [3]. As our setup allows for a wide range of object and reference angle combinations, a quantitative evaluation of every writable angle is not feasible. This is because the aspired VCA consists of 4096 different reference and object angle combinations, whose individual measurement regarding efficiency and spectral distribution is too much time consuming. The holographic printer itself is fully automized, but efficiency and spectral measurements are still done manually.

As a more tangible approach, we optimized for printing parameters at a fixed object angle and fixed azimuth angles φ, but different elevation angles θ of the reference beam. The optimal parameters for each θ are found by printing single cells with variation in exposure time and laser power. Based on the obtained data, the optimal printing parameters for other reference angles are calculated by making use of Equation (15). The achieved diffraction efficiencies depending on different elevation angles θ are given in Figure 7, together with the optimal beam ratio.

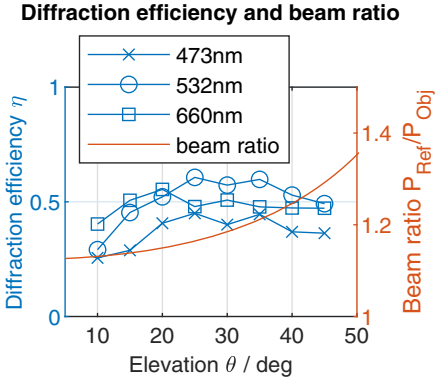

Figure 7: Diffraction efficiency of single hogels with increasing elevation angles θ and the optimal beam ratio due to Fresnel reflection.

Despite variation of θ and laser wavelength, the efficiency of the printed cells stays nearly constant at $\eta \approx 0,5$. The diffraction efficiency is calculated by measuring the diffracted and transmitted beam power P_D and P_T

$$\eta = \frac{P_D}{P_D + P_T}. \tag{17}$$

Higher efficiencies of $\eta > 0,9$ should be possible, as shown in the study by Berneth et al. [14], but could not be achieved in consequence of a not ideal surface quality of the parabolic reflector.

3.2 Test of a collimating VCA

To demonstrate the purpose of our setup, a collimating VCA is produced in form of a reflection hologram for an LED that is positioned at a distance of 40 mm and with an angle of $\theta_0 = 50$ deg to the VCA, as depicted in Figure 1. In case of collimation, the object beam is fixed (parallel light beam), while the reference beam changes in θ and φ to match the beam characteristics of the LED. Pseudocolor images of the resulting angle distributions of the VCA are shown in Figure 8. The VCA has a border width of 41, 9 mm containing 64×64 individual cells. As the active area of the lightsource has an edge length of approximately 1 mm, the different reference angles converge to the center of the lightsource, which is positioned at the center of the y axis on the left side in negative x direction from the view of Figure 8.

If the reference angle distribution indeed matches the LED characteristics, the lightrays are deflected similar to the object beam, which yields a parallel light beam. The VCA is then produced by printing all 4096 cells individually in an automated process: The reference angle is changed for every cell according to the values in Figure 8, the described corrections are executed and the substrate is moved to the right position. After that the film is being exposed within the dimension of a single cell.

Figure 9 shows the light distribution generated by the VCA under LED illumination. As the LED is positioned to the left side of the VCA, the intensity on the left side is

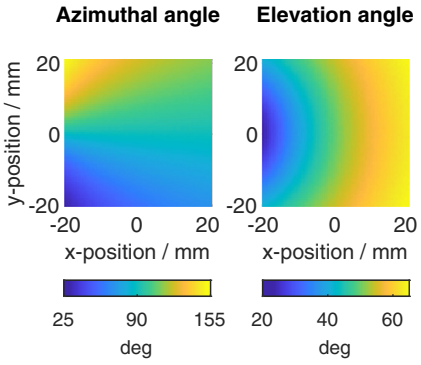

Figure 8: Pseudocolor images of the reference beam angle distribution of the collimating VCA with azimuth φ and elevation θ.

bigger due to the quadratic distance law and a gradient in the distribution is visible. Because the VCA has a quadratic shape, the ideal distribution would be quadratic as well. The screen is positioned in L=545 mm distance beyond the VCA and the square-shaped distribution has an approximate width of $\Delta x \approx 100$ mm which results in a remaining divergence of

$$\omega_{\text{div}} = \arctan\left(\frac{\Delta x}{2 \cdot L}\right) \approx 5\,\text{deg}. \tag{18}$$

The spectral distribution of the LED, the VCA and the laser wavelength during manufacturing can be seen in Figure 10. The used laser has a wavelength of $\lambda_{L_1} = 532$ nm, therefore the VCA lies in the green spectral range. Shrinkage of the material during the manufacturing process is below 3% [3], but causes a spectral shift of the reflected light toward shorter wavelengths. The angle distribution in Figure 8 shows that the VCA acts similar to an off-axis parabolic mirror for green light. As the reconstruction angle θ decreases after shrinkage, but the azimuthal direction is different for each cell, the result can be compared to a slight deformation of the off-axis parabolic mirror, which explains the aberrations visible in the target distribution.

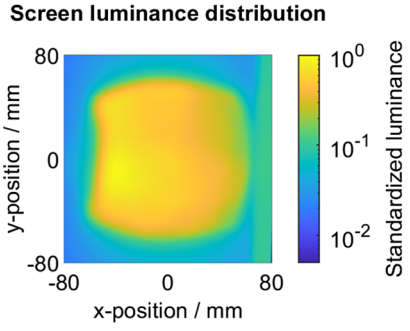

Figure 9: Standardized luminance distribution of the VCA on the screen depicted in Figure 1.

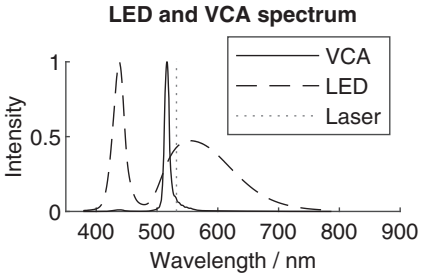

Figure 10: Spectrum of the LED, the VCA light distribution on the screen and the wavelength of the laser used during manufacturing.

4 Summary and outlook

In this article, we presented a new setup for the fabrication of volume holographic cell arrays in transparent photopolymer films. Key aspect of the setup is the variation of the reference angle within the hologram matrix using a parabolic mirror. The aim is to create very thin optical elements capable of forming light distributions with incoherent lightsources like LEDs. Current approaches for printing matrix holograms focus on increasing the quality of image reconstruction by decreasing the pixel size of the matrix or overlapping of the matrix elements[15, 16]. Hofmann et al. are printing holographic diffusers [17] or micromirror arrays [18] utilizing a holographic printer with two SLMs allowing for arbitrary wavefronts being depicted onto each side of the holographic film. Yet the reconstruction of these vHOE is done with collimated light or laser beams, which requires preshaping of the lightsource, especially when LEDs are used for illumination at small distances.

With our setup, we pursue the approach to adapt matrix holograms to the specific radiation characteristics of arbitrary lightsources, which will render preshaping obsolete. As a first step, we managed to produce a reflection hologram, collimating the green spectral segment of an LED to a remaining divergence of $\omega_{\text{div}} \approx 5$ deg. In the study by Neumann and Giehl [19], we presented an approach to redistribute light with VCAs to form light distributions while using incoherent light sources. To this end, the principle was only shown for collimated LEDs. This setup allows for the next steps to be the combination of the light redistribution applied to the object beam with the demonstrated collimation accomplished by the reference beam variation. In combination, it might be possible to digitally tailor VCAs to a specified lightsource, thereby creating VCAs for different types of LEDs without changing the printer setup and enabling holograms to be used as illumination optics.

Author contribution: All the authors have accepted responsibility for the entire content of this submitted manuscript and approved submission.
Research funding: None declared.
Conflict of interest statement: The authors declare no conflicts of interest regarding this article.

References

[1] D. Gabor, "Associative holographic memories," *IBM J. Res. Dev.*, vol. 13, no. 2, pp. 156–159, 1969.
[2] M. Liebling, T. Blu, E. Cuche et al., "A novel non-diffractive reconstruction method for digital holographic microscopy," in *Proceedings IEEE International Symposium on Biomedical Imaging*, Washington, DC, USA, 2002, pp. 625–628.
[3] F. K. Karl Bruder, T. Fäcke, and T. Rölle, "The chemistry and physics of bayfol® hx film holographic photopolymer," *Polymers*, vol. 9, no. 10, p. 472, 2017.
[4] M. Mügge and C. Smarslik, "New technologies shift 3d-lighting onto a higher level," in *ISAL*, vol. 17, 2017, pp. 63–72.
[5] W. Henry Bragg and W. Lawrence Bragg, "The reflection of x-rays by crystals," *Proc. R. Soc. Lond. - Ser. A Contain. Pap. a Math. Phys. Character*, vol. 88, 1913, no. 605, pp. 428–438.
[6] H. Kogelnik, "Coupled wave theory for thick hologram gratings," in *Landmark Papers On Photorefractive Nonlinear Optics*, Singapore, World Scientific, 1995, pp. 133–171.
[7] F-K. Bruder, H. Bang, T. Fäcke, et al., "Precision holographic optical elements in bayfol hx photopolymer," in *Practical Holography XXX: Materials and Applications*, vol. 9771, 2016, p. 977103.
[8] G. D. Mintz, D. K. Morland, and W. M. Boerner, "Holographic simulation of parabolic mirrors," *Appl. Optic.*, vol. 14, no. 3, pp. 564–565, 1975.
[9] D. Karthaus, M. Giehl, O. Sandfuchs, and S. Sinzinger, "Optimization of computer generated transmission holograms using led wave front approximations," in *DGaO Proceedings*, Dresden, Germany, 2017, p. A8.
[10] D. Karthaus, M. Giehl, O. Sandfuchs, and S. Sinzinger, "Modeling of light-emitting diode wavefronts for the optimization of transmission holograms," *Appl. Optic.*, vol. 56, no. 18, pp. 5234–5241, 2017.
[11] M. Andrulevičius, T. Tamulevičius, and S. Tamulevičius, "Formation and analysis of dot-matrix holograms," *Mater. Sci.*, vol. 13, no. 4, pp. 278–281, 2007.
[12] F.-K. Bruder, F. Deuber, T. Fäcke, et al., "Reaction-diffusion model applied to high resolution bayfol hx photopolymer," in *Practical Holography XXIV: Materials and Applications*, vol. 7619, 2010, Art no. 76190I.
[13] B. E. A. Saleh and Malvin Carl Teich. *Grundlagen der Photonik*, Weinheim, Germany Wiley-VCH, 2008.
[14] H. Berneth, F.-K. Bruder, T. Fäcke, et al., "Holographic Recordings with High Beam Ratios on Improved Bayfol® Hx Photopolymer," in *Holography: Advances and Modern Trends III*. International Society for Optics and Photonics, 2013, p. 8776.
[15] K Wakunami, R. Oi, T. Senoh, et al., "Wavefront printing technique with overlapping approach toward high definition holographic image reconstruction," in *Three-Dimensional Imaging, Visualization, and Display 2016*, Baltimore, Maryland, United States, vol. 9867, International Society for Optics and Photonics, 2016, p. 98670J.
[16] Y. Ichihashi, K. Yamamoto, K. Wakunami, et al., "An analysis of printing conditions for wavefront overlapping printing," in *Practical Holography XXXI: Materials and Applications*, vol. 10127, San Francisco, California, United States, International Society for Optics and Photonics, 2017, p. 101270L.
[17] J. Hofmann, R. Fiess, M. Kick, W. Stork, "Extended holographic wave front printer setup employing two spatial light modulators," in *Holography: Advances and Modern Trends VI*, vol. 11030, Prague, Czech Republic, International Society for Optics and Photonics, 2019, p. 110300N.
[18] J. Hofmann, R. Fiess, and W. Stork, "Holographic wave front printing for fabrication of reflection holograms with arbitrary recording wave fronts," in *Practical Holography XXXIV: Displays, Materials, and Applications*, vol. 11306, San Francisco, California, International Society for Optics and Photonics, 2020, p. 1130602.
[19] C. Neumann, M. Giehl, "Volume holographic grating cell arrays for illumination purposes," in *DGaO Proceedings*, vol. 7619, Darmstadt, Germany, 2019, p. C9.